



1 **Optical and molecular-level characterization of fluvial organic**  
2 **matter biodegradation in a highly urbanized river system**

3 Most Shirina Begum<sup>1</sup>, Hyojin Jin<sup>1</sup>, Inae Jang<sup>2</sup>, Jung-Min Lee<sup>2</sup>, Han Bin Oh<sup>2</sup>, Ji-Hyung Park<sup>1</sup>

4 <sup>1</sup>Department of Environmental Science & Engineering, Ewha Womans University, Seoul 03760, Republic of Korea

5 <sup>2</sup>Department of Chemistry, Sogang University, Seoul 04107, Republic of Korea

6 *Correspondence to:* Ji-Hyung Park (jhp@ewha.ac.kr); Han Bin Oh (hanbinoh@sogang.ac.kr)



7 **Abstract.** Rapid urbanization worldwide is changing both the transport of organic matter (OM) and CO<sub>2</sub> emission in urban  
8 streams and rivers, yet little is known as to how the altered quality of riverine OM affects biodegradation and CO<sub>2</sub> emission.  
9 The relationships between the chemical properties and biodegradation of riverine OM, including dissolved and particulate  
10 OM (DOM and POM), were examined against the level of anthropogenic perturbation along the Han River, a river system in  
11 South Korea that has been highly modified by dams and urban water pollution. DOM optical properties and biodegradable  
12 dissolved organic carbon (BDOC), together with in situ measurements of the partial pressure of CO<sub>2</sub> (*p*CO<sub>2</sub>) using a  
13 membrane-enclosed sensor, were compared between the up-, mid-, and downstream reaches of the Han River and three  
14 urban tributaries in a basin-scale field campaign combined with a 7 day incubation of both filtered and unfiltered samples.  
15 Another 5 day incubation was conducted with unfiltered water samples from a downstream river site and an urban tributary,  
16 in isolation and mixed (1:1), to measure changes in dissolved CO<sub>2</sub> concentrations at 10-min intervals and BDOC and optical  
17 properties at intervals of 1–2 days. Fourier transform-ion cyclotron resonance-mass spectrometry (FT-ICR-MS) was used to  
18 detect molecular-level changes in DOM composition between the initial and post-incubation samples. The average BDOC  
19 concentration in the urban tributaries was 4–12 times higher than those of three mainstem reaches, while BDOC was highly  
20 variable at three downstream sites and tended to be higher at the mainstem sites affected by agricultural runoff or dams than  
21 at the forested headwater stream. Longitudinal increases in protein-like and “microbial” humic-like fluorescence,  
22 fluorescence index (FI), and biological index (BIX) reflected increasing inputs of anthropogenic DOM along the  
23 downstream reach and urban tributaries. These optical indices, along with *p*CO<sub>2</sub>, were significantly correlated with BDOC  
24 concentrations measured at 12 sites. The cumulative CO<sub>2</sub> production measured in the second incubation was greatest in the  
25 mixture, followed by the urban tributary and mainstem samples in the descending order. The amount of CO<sub>2</sub> produced in the  
26 mixture was greater than the BDOC measured in the same sample or the average of CO<sub>2</sub> produced in the separate samples,  
27 indicating a mixing-enhanced biodegradation of DOM including the fraction transformed from soluble components of POM.  
28 FT-ICR-MS analysis revealed a much larger number of molecules consumed (3984) than those produced (771) during the  
29 incubation of the mainstem sample in contrast to the produced molecules (2789) exceeding the consumed molecules (1479)  
30 in the tributary sample, indicating a high rate of OM processing in the urban tributary that might be limited in the  
31 availability of immediately consumable organic materials. Overall results suggest that water pollution, along with  
32 impoundment effects of dams, can alter the optical properties and biodegradability of both DOM and POM in highly  
33 urbanized watersheds to such a degree that can induce a priming effect on OM biodegradation and CO<sub>2</sub> emission.



34 **Key words:** biodegradation; CO<sub>2</sub> emission; dissolved organic matter; fluorescence EEMs; FT-ICR-MS; particulate organic  
35 matter; urbanized watershed; water pollution

## 36 **1 Introduction**

37 Inland waters, as a crucial component of the global carbon cycle, can provide a positive feedback to climate change, because  
38 active transformations of organic matter (OM) of both terrestrial and aquatic origin during transit to the oceans result in  
39 large emissions of CO<sub>2</sub> and CH<sub>4</sub> (Aufdenkampe et al., 2011; Bastviken et al., 2013; Cole et al., 2007; Raymond et al., 2013;  
40 Wehrli, 2013). Transformations of OM in inland waters can be affected by concurrent changes in climatic conditions,  
41 agricultural activities, water impoundments, and other anthropogenic modifications of water flow and quality in increasingly  
42 urbanizing watersheds worldwide (Casas-Ruiz et al., 2016; Hutrya et al., 2014; Kaushal et al., 2014; Parr et al., 2015;  
43 Regnier et al., 2013). In eutrophic inland waters receiving high loads of anthropogenic OM, enhanced transformations of  
44 OM and subsequent changes in chemical characteristics have been explored by employing various OM characterization  
45 techniques including absorbance and fluorescence measurements (Abril et al., 2002; Baker, 2001; Hosen et al., 2014;  
46 Williams et al., 2016; Wilson and Xenopoulos, 2009). Increased biodegradability in urbanized watersheds has been linked to  
47 increased inputs of labile OM from anthropogenic sources and an associated potential enhancement of the biodegradation of  
48 natural organic materials (Guo et al., 2014; Knapik et al., 2015; Parr et al., 2015). Recent studies have quantified and  
49 characterized increasing loads of dissolved OM (DOM) in urbanized rivers and estuaries (Guo et al., 2014; Hosen et al.,  
50 2014; McElmurry et al., 2014; Parr et al., 2015). However, the characterization of DOM has rarely been associated with  
51 altered rates of greenhouse gas (GHG) emissions from urbanized river systems (Kaushal et al., 2014).

52 Optical characterization of DOM has been used to examine land use effects on the quality of DOM in streams and rivers  
53 draining agricultural lands (Petrone et al., 2011; Wilson and Xenopoulos, 2009) and urban population centers (Hosen et al.,  
54 2014; McElmurry et al., 2014). DOM absorbance and related indices such as specific absorbance at 254 nm (SUVA<sub>254</sub>),  
55 absorbance coefficients based on absorbance measurements at 254 nm ( $a_{254}$ ) and 350 nm ( $a_{350}$ ), spectral slopes over the  
56 ranges of 275-295 nm ( $S_{275-295}$ ) and 350-400 nm ( $S_{350-400}$ ) and slope ratio ( $S_R$ ) have frequently been used as efficient tools for  
57 optical characterization of DOM (Helms et al., 2008; Spencer et al., 2012). Fluorescence excitation-emission matrices  
58 (EEMs) can visualize fluorescent DOM (FDOM) components that can indicate the source and biodegradability of DOM  
59 (Baker, 2001; Osburn et al., 2012). Fluorescence indices such as fluorescence index (FI) (McKnight et al., 2001),



60 humification index (HIX) (Zsolnay et al., 1999), and biological index (BIX) (Huguet et al., 2009; Parlanti et al., 2000),  
61 along with various FDOM components including “terrestrial” and “microbial” humic-like fluorescence and protein-like  
62 fluorescence and their ratios (Fellman et al., 2010), have been used to examine the source and lability of DOM in a wide  
63 range of inland waters. Biodegradable dissolved organic carbon (BDOC) has been shown to increase in urbanized river  
64 systems (Knapik et al., 2015; Shi et al., 2016) and agricultural watersheds (Royer and David, 2005; Stanley et al., 2011);  
65 however, there have been only a few studies that examined the relationships between BDOC and optical properties of DOM  
66 in highly human-modified streams and rivers (e.g., Hur et al., 2014a; Parr et al., 2015). Recent studies have used Fourier  
67 transform-ion cyclotron resonance-mass spectrometry (FT-ICR-MS) to provide molecular-level information on  
68 compositional changes incurred from DOM biodegradation (Ward et al., 2013), opening a new way to investigate the  
69 relationships between the chemical characteristics and biodegradability of DOM.

70 The priming effect has recently been proposed as a possible explanation for large CO<sub>2</sub> emissions from inland water systems  
71 and the lack of recalcitrant terrigenous components in marine sediments (Bianchi, 2011; Bianchi et al., 2015). The concept  
72 of priming effect was originally used in the study of soil OM to explain enhanced decomposition of recalcitrant organic  
73 materials following the addition of labile materials (Kuzyakov et al., 2000). Recent applications to the study of inland waters  
74 have provided contrasting results, including negative priming, no priming, and positive priming (Bianchi et al., 2015;  
75 Catalan et al., 2015; Guenet et al., 2014; Hotchkiss et al., 2014; Kuehn et al., 2014). Rare efforts have yet been made to  
76 examine priming effects of anthropogenic pollution or algal OM produced in impounded reaches in highly modified river  
77 systems. Furthermore, previous studies of priming effects on riverine OM biodegradation have not adequately addressed  
78 active transformations between DOM and particulate OM (POM) driven by microbial assimilation and degradation (Osburn  
79 et al., 2012; Ward et al., 2013). Combining continuous CO<sub>2</sub> measurements with BDOC quantification can enable a more  
80 accurate assessment of the priming effect induced by inputs of labile OM components (Bianchi et al., 2015). The primary  
81 aim of this study was to examine the relationships between optical characteristics and biodegradability of DOM and POM in  
82 the Han River watershed, which has a large spatial diversity ranging from the predominantly forested upstream reach  
83 through the heavily impounded midstream reach to the highly urbanized downstream reach receiving high loads of  
84 anthropogenic OM from urban tributaries. Another goal was to investigate whether priming effects of labile OM of  
85 autochthonous or anthropogenic origin can enhance the rate of biodegradation of riverine OM and hence CO<sub>2</sub> emission from  
86 the eutrophic urban river. A basin-scale field survey was combined with two laboratory incubation experiments to provide



87 more detailed understanding of how downstream changes in riverine OM quality driven by dams and urban water pollution  
88 can enhance the biodegradation of DOM, with and without POM, either in the field or in controlled laboratory settings.

## 89 **2 Materials and methods (Will be shortened after English editing)**

### 90 **2.1 Study site and basin-scale survey**

91 The Han River basin (36°30' to 38°55' N; 126°24' to 129°02' E) consists of two main branches – the North Han River and  
92 the South Han River – and the lower Han River along the Seoul metropolitan area (Fig. 1) (Chang, 2008; Hur et al., 2014b).  
93 Surface water samples were collected along the longitudinal continuum encompassing the North Han River and the lower  
94 Han River (Fig. 1; Table S1). The river runs 515 km along the waist of the Korean Peninsula from the heavily forested  
95 headwaters in Gangwon province to the Seoul metropolitan area with more than 25 million residents, draining a total area of  
96 26,018 km<sup>2</sup> (Ministry of Environment Korea). In the upstream reach of the North Han River, about 87 % of the watershed is  
97 covered with forests, 7 % with agricultural farm lands, and 2 % with residential areas (Kang and Park, 2015; WAMIS).  
98 Expansion of agricultural lands on steep mountainous terrain over the recent decades has increased rates of soil erosion,  
99 often resulting in large exports of sediments and associated POM during intense storm events (Jung et al., 2015). Along the  
100 midstream reach of the North Han River, 68 %, 13 %, and 15 % of the watershed is covered with forests, agricultural farm  
101 lands, and residential areas respectively (Kang and Park, 2015; WAMIS, 2006). In addition to the effect of agricultural farm  
102 lands, four large dams along the midstream reach of the North Han River affect the water quality by increasing the mean  
103 water retention time (Jung et al., 2014; MOLIT, 2016). Along the downstream reach of the Han River from the outflow of  
104 the Lake Paldang to the Yellow Sea, forests and agricultural lands each account for about 31 % and the residential areas  
105 25 % of the watershed (Chang, 2008; Kang and Park, 2015; WAMIS). The flow of the lower Han River is strongly affected  
106 by discharges from the Lake Paldang and two in-stream weirs constructed in the upper and lower ends of the river section  
107 along the city of Seoul (Kang and Park, 2015; Yoon et al., 2010). Three major urban tributaries, together with other small  
108 streams, deliver discharges from waste water treatment plants (WWTP) and urban runoffs into the downstream reach of the  
109 Han River (Fig. 1).

110 To examine spatial variations in the optical characteristics and biodegradability of riverine OM across the North Han River  
111 basin and the lower Han River, water samples were collected from three upstream, three midstream, and three downstream  
112 locations of the Han River, and three urban tributaries along the downstream reach in May 2015 (Fig. 1; Table S1). Spot



113 samples were collected into acid-washed glass bottles from a depth of 10–20 cm below the water surface using a portable  
114 water sampler (Masterflex E/S, Cole-Parmer, Illinois, USA). Samples were transported on ice to the laboratory. Subsamples  
115 that were filtered within 1–2 days after sampling, together with unfiltered subsamples, were stored at 4°C until chemical  
116 analyses including BDOC determination.

117 During water sampling, in situ measurements of the partial pressure of CO<sub>2</sub> ( $p\text{CO}_2$ ) were conducted at the same water depth  
118 using a CO<sub>2</sub> sensor (CARBOCAP®, GMT222, Vaisala, Finland) enclosed in PTFE-membrane (200-07, International  
119 Polymer Engineering, USA). The method is described in detail in Yoon et al. (2016). The sensor system includes two CO<sub>2</sub>  
120 sensors for concurrent measurements of water and atmospheric  $p\text{CO}_2$ , a data logger (CR10X, Campbell Scientific Inc.,  
121 USA), and three batteries (12 V 7 AH, Rocket, Korea). Before the sampling, the CO<sub>2</sub> sensors were calibrated in the  
122 laboratory using CO<sub>2</sub> standard gases of known concentrations (0, 500, 5000, 10000 ppm). The sensor output was corrected  
123 for the ambient pressure; values were increased or decreased by 0.15 % for 1 hPa decrease or increase in pressure from the  
124 standard pressure used for calibration, respectively (Johnson et al., 2010). The output was also corrected for temperature:  
125 0.3 % increase or decrease for 1 °C higher or lower temperature than the standard temperature used for calibration,  
126 respectively (Johnson et al., 2010).

## 127 **2.2 Seven-day laboratory incubation**

128 A 7 day laboratory incubation was conducted with the water samples collected at 12 sampling locations along the Han River  
129 and urban tributaries (Fig. 1), following the methods modified from Servais et al. (1987) and Wickland et al. (2012). A  
130 subset of samples were filtered through pre-combusted glass fiber filters (GF/F, Whatman; nominal pore size 0.7 µm) to  
131 remove POM. Three replicates of the filtered sample (80 ml) were incubated in 120 ml amber glass bottles at 20 °C (the  
132 average water temperature during sampling) in the dark. A small volume (1 % of each incubated water sample) of the  
133 original, unfiltered water sample was added as a site-specific inoculum to the respective incubation sample to provide  
134 indigenous microorganisms that can degrade DOM components in the filtered water sample. Another batch of unfiltered  
135 samples was incubated under the same conditions without addition of any inoculum to compare additional effects of POM  
136 on riverine OM biodegradation. To maintain aerobic condition in the closed incubation bottles throughout the incubation  
137 period, the bottles were uncapped and gently shaken for 30 min every two days. BDOC was calculated as the difference  
138 between the final and initial concentrations of DOC. Another set of samples containing only ultrapure water (Milli-Q,



139 Millipore, MA, USA) was also included as a control to observe any contamination or analytical errors.

### 140 **2.3 Five-day laboratory incubation**

141 To investigate priming effects of anthropogenic or autochthonous OM on the biodegradation of riverine OM in the  
142 downstream reach under more realistic water conditions considering both DOM and POM, the second incubation  
143 experiment was conducted with unfiltered water samples from an upstream location of the lower Han River, ~ 20 km  
144 downstream of the Lake Paldang (hereafter termed “mainstem”) and an urban tributary, Jungnang Stream (hereafter termed  
145 “tributary”) (Fig. 1). Samples were collected in acid-washed 20 L polycarbonate containers in July 2015 from 10 –20 cm  
146 below the surface of the mainstem and tributary using a portable water sampler. A mixture sample (hereafter termed  
147 “mixture”) was prepared by mixing the samples from the Han River mainstem and the urban tributary with a mixing ratio of  
148 1:1. In one experimental set-up, replicates of 60 ml unfiltered samples were placed in acid-washed amber glass bottles (120  
149 ml). The bottles were sealed with butyl septa and aluminum crimps and then incubated for five days, with three bottles per  
150 treatment destructively sampled at 0 h, 1 h, 1 day, 3 day, and 5 day. A prior test had shown that a larger headspace volume  
151 than the first experiment could maintain aerobic condition in the closed bottles for 5 days. Samples were incubated in the  
152 dark at 25 °C, which was the average water temperature during the month when water samples were collected. In another  
153 experimental set-up, one 10 L sample per treatment was incubated in 20 L gas-tight polycarbonate containers; the same  
154 50 % headspace volume was created to maintain aerobic condition within the sealed incubation container. A membrane-  
155 enclosed CO<sub>2</sub> sensor that had been used in the field survey was immersed in each of three samples in order to measure  
156 dissolved CO<sub>2</sub> in the water at 10 min intervals. The sensor output in *p*CO<sub>2</sub> values were converted to dissolved CO<sub>2</sub>  
157 concentrations (mg C L<sup>-1</sup>) using Henry’s constant for dissolved CO<sub>2</sub> at standard temperature and pressure (Johnson et al.,  
158 2010).

### 159 **2.4 Chemical analysis**

160 Water samples were filtered through pre-combusted glass fiber filters to remove suspended materials. Concentration of total  
161 suspended solid (TSS) were measured gravimetrically as the difference in the filter weight before and after filtering and  
162 drying at 60 °C for 48 hours. The concentration of DOC was measured using a total organic carbon (TOC) analyzer using  
163 high-temperature combustion of OM followed by thermal detection of CO<sub>2</sub> (TOC-V<sub>CPH</sub>, Shimadzu, Japan). As part of



164 quality control, standards with known DOC concentrations and ultrapure water were analyzed for every batch of ten samples  
165 and triplicate analysis was performed for approximately 10 % of all analyzed samples to assess instrumental stability and  
166 accuracy.

167 Fluorescence EEMs were collected on a fluorescence spectrophotometer (F7000, Hitachi, Japan) by simultaneous scanning  
168 over excitation wavelengths from 200 to 400 nm at 5 nm interval and emission wavelengths from 290 to 540 nm at 1 nm  
169 interval. Scan speed was 2400 nm min<sup>-1</sup> and the bandwidth was set to 5 nm for both excitation and emission. A 290 nm  
170 cutoff filter was used for all the measurements to minimize second-order Rayleigh scattering. Blank run with ultrapure water  
171 was conducted at least once for every batch of 10 samples and Raman band intensity at Ex. 350 nm/Em. 400 nm was used to  
172 monitor the instrumental stability. Fluorescence intensities of the actual water samples were divided by the Raman band  
173 intensity determined prior to sample measurements to correct any fluctuation in instrumental conditions. All the EEMs were  
174 corrected for the Rayleigh scattering and inner-filter effect by subtracting the blank measurements from the sample  
175 measurements and by using an absorption-based correction equation suggested by Ohno (2002), respectively. UV  
176 absorbance was measured across the wavelength range from 200 to 1100 nm using a UV-Vis spectrophotometer (Agilent  
177 8453, USA).

178 Optical fluorescence parameters were obtained from the corrected EEMs and absorbance values at the respective  
179 wavelengths (Table S2). Optical indices such as HIX (Zsolnay et al., 1999), FI (McKnight et al., 2001), and BIX (freshness  
180 index or  $\beta:\alpha$  ratio) (Parlanti et al., 2000; Wilson and Xenopoulos, 2009) were obtained from the EEMs (Table S2).  
181 Fluorescence intensities of three FDOM components, including “terrestrial” humic-like FDOM (C1) associated with soil-  
182 derived humic substances, “microbial” humic-like FDOM (C2) indicating autochthonous OM produced by microbial activity,  
183 and protein-like FDOM (C3) derived from microbial metabolites of natural or anthropogenic OM were also obtained for the  
184 wavelength ranges identified in the same study site and other studies (Table S2; Fellman et al., 2010). In addition, absorption  
185 parameters such as  $a_{254}$ ,  $a_{350}$ ,  $SUVA_{254}$ ,  $SUVA_{350}$ ,  $S_{275-295}$ ,  $S_{350-400}$  were determined from UV absorbance measurements  
186 (Table S2; Helms et al., 2008; Weishaar et al., 2003).

## 187 **2.5 Acquisition and analysis of FT-ICR mass spectra**

188 Solid phase extraction (SPE) was used to extract DOM from a large volume (5 L) of the mainstem and tributary samples  
189 before and after the 5 day incubation, following Dittmar et al. (2008). The mixture sample was not included due to logistical



190 constraints. Samples were filtered (GF/F; 0.7  $\mu\text{m}$ ) and acidified to pH 2 using 30 % HCl right before SPE in order to  
191 enhance extraction efficiency. Precipitation of DOM due to acidification was not observed in any of the samples. PPL  
192 cartridges (Agilent Technologies Inc., Santa Clara, CA, USA) of 6 ml volume with 1 g sorbent were used for DOM  
193 extraction. Cartridges were rinsed with 12 ml of methanol (99.8 %) and 1 L of Milli-Q water to remove any potential OM  
194 contamination. Samples were passed through the cartridge using a peristaltic pump at a flow rate of 20 to 30 ml  $\text{min}^{-1}$ .  $\text{N}_2$   
195 gas was purged slowly to dry the cartridge. DOM was extracted by passing 6 ml of methanol very slowly, approximately at  
196 the rate of 1 ml  $\text{min}^{-1}$ . Samples were collected and stored in a 10 ml glass ampule and stored at  $-20\text{ }^\circ\text{C}$  until FT-ICR-MS  
197 analysis. Samples were purged with  $\text{N}_2$  gas to increase the concentration of DOM for FT-ICR-MS analysis.

198 Ultrahigh resolution mass spectra were acquired using a 15 Tesla Fourier transform ion cyclotron resonance (FT-ICR) mass  
199 spectrometer (Solarix, Bruker Daltonics Inc., Billerica, MA, USA), equipped with an Apollo II ion funnel electrospray  
200 ionization (ESI) source, at Korea Basic Science Institute (KBSI, Cheongju, Korea). ESI mass spectra of DOM were obtained  
201 in negative ion mode. A DOM sample solution dissolved in methanol:water 1:1 (v/v) with 0.1 % ammonium hydroxide (pH  
202  $\sim 8$ ) was infused continuously at a flow rate of 120  $\mu\text{L h}^{-1}$  using a syringe pump (Harvard Apparatus, Holliston, MA, USA).  
203 Drying gas temperature was set to 210  $^\circ\text{C}$  and its flow rate was 4.0 L  $\text{min}^{-1}$ . Electrosprayed ions (spray voltage: -3.0 kV)  
204 were introduced into the mass spectrometer and externally accumulated for  $\sim 0.5$  s in order to increase detected ion  
205 abundance, and then transferred to the ICR cell. FT-ICR mass spectra were acquired over 100 time-domain transients at 4  
206 Mword over the mass range of  $m/z$  160/1000 in broadband mode. All the samples were analyzed in triplicates. The summed  
207 free induction decay signal was zero-filled once and full-sine apodized prior to fast Fourier transform processing.

208 FT-ICR MS spectra were calibrated externally and internally using a series of arginine (Sigma, St. Louis, MO, USA)  
209 clusters in negative ion mode. The ion peaks were selected with a criterion of S/N ratio of  $\geq 5$  and a peak list was generated.  
210 The ion peaks detected at least two times out of triplicate measurements were included in the peak list. All the detected ions  
211 were singly charged (assumed to be deprotonated), which was confirmed by the isotope spacing. The ion peak abundances  
212 were normalized with respect to the sum of all the ion abundances. Chemical formula assignment was performed with self-  
213 written software and database that were coded with MATLAB (MathWorks, Inc., Natick, MA, USA). The home-coded  
214 software was rigorously validated using the data provided in the supporting information of Koch et al. (2007). The database  
215 was constructed following the stringent criteria with elemental combinations of  $^{12}\text{C}_{1-100}$   $^1\text{H}_{0-200}$   $^{16}\text{O}_{1-50}$   $^{14}\text{N}_{0-10}$   $^{31}\text{P}_{0-2}$   $^{32}\text{S}_{0-2}$ . In  
216 the database, the chemical formula entities that violate the nitrogen rule and double bond equivalent rule were all eliminated



217 (Koch et al., 2007; McLafferty and Turecek, 1993). In addition, the chemical formula entities were further selected to meet  
218 the following elemental ratio criteria:  $0.3 < H/C < 2.25$ ,  $O/C < 1.0$ ,  $N/C < 1.0$ ,  $S/C < 0.2$ ,  $H \leq 2C+N+P+2$ ,  $P/C < 0.1$ ,  $S+P/C <$   
219  $0.2$ ,  $O \leq C+2$  (Koch et al., 2007; Stubbins et al., 2010). The formulas containing  $N_2S_2$  were all removed from the  
220 database. Further, when a homologous series with relative peak distances of 36.4 mDa were detected, the so-called  
221 “chemical building block” approach was adopted in order to unambiguously assign the ion peaks (Koch et al., 2007). In  
222 database search, the mass accuracy limit was set to be less than 1 ppm. Van Krevelen plots were drawn using MATLAB  
223 software.

## 224 2.6 Statistical analysis

225 Paired t-test was performed to identify any significant difference in BDOC concentration and other optical measurements  
226 between the filtered and unfiltered samples from the field survey and the first incubation experiment. Paired t-test was also  
227 used to identify significant differences in optical measurements between the initial and post-incubation samples. Regression  
228 analysis was conducted to establish significant relationships between BDOC and other measurements at 12 sites. Analysis of  
229 variance (ANOVA) followed by Tukey’s honest significant difference (HSD) was used to examine significant differences  
230 among the up-, mid-, and downstream reaches, and the urban tributaries. Normality of data distribution was examined prior  
231 to conducting paired t-test and ANOVA and any data sets showing non-normal distribution were normalized by log-  
232 transformation of the data. All analyses were conducted on R software environment for statistical computing and graphics  
233 (R Development Core Team, 2011). Unless otherwise noted, all reported significance levels were set at  $P < 0.05$ .

## 234 3 Results

### 235 3.1 Basin-scale spatial patterns of optical properties and biodegradability of DOM and POM

236 The  $pCO_2$  measured in situ was much higher at two urban tributary sites (4,342 and 11,449  $\mu\text{atm}$ ) than at the river mainstem  
237 sites and exhibited downstream increases from the generally low values across the up- and mid-stream sites ( $<1,000 \mu\text{atm}$ )  
238 to the medium-range values at the downstream sites (Fig. 2; Table S3b). The concentrations of BDOC measured during the 7  
239 day incubation with both filtered and unfiltered samples from 12 sites showed distinct spatial patterns (Fig. 2; Table S3). The  
240 highest BDOC value was observed for an urban tributary ( $1.01 \text{ mg C L}^{-1}$ ; 20 % of the initial DOC) and the lowest BDOC in  
241 the forested headwater stream ( $0.01 \text{ mg L}^{-1}$ ; 1.4 % of the initial DOC), with an average %BDOC of 10 % for all samples.



242 Average BDOC concentrations at the urban tributaries ( $0.82 \pm 0.18 \text{ mg C L}^{-1}$ ) were 4–12 times higher than those measured  
243 across three mainstem reaches (Fig. 2; Table S3). BDOC concentrations at a midstream (Mid 3) and a downstream (Down 2)  
244 sites and two urban tributaries (Urban 1, 2) were slightly, but significantly higher in the unfiltered samples compared to the  
245 filtered samples.

246 Fluorescence intensities of three fluorescence EEM components (C1, C2, and C3) measured for the initial samples prior to  
247 the incubation exhibited downstream increases with the highest values at the urban tributaries (Fig. 3; Table S3a). Ratios  
248 among the three FDOM components, i.e., C2/C1, C3/C1, and C3/C2, tended to be higher at the downstream and urban  
249 tributary sites compared to the up- and midstream sites. HIX was distinctly higher at the upstream sites and remained  
250 relatively small from the midstream to tributary sites, whereas FI and BIX increased gradually from the upstream sites  
251 toward the urban tributaries. Regression analyses revealed significant positive relationships between BDOC and many  
252 measured variables including  $p\text{CO}_2$ , DOC,  $a_{254}$ ,  $a_{350}$ , C1, C2, C3, and FI (Fig. 4). Over the 7 day incubation, C3 and its ratios  
253 to C1 and C2 showed significant decreases at the downstream and tributary samples (Fig. S1a), whereas  $a_{350}$ ,  $\text{SUVA}_{254}$ , and  
254  $S_g$  increased significantly at the downstream samples (Fig. S1b).

255 Fluorescence EEMs measured for the initial water samples exhibited pronounced downstream changes in the shape and  
256 intensity of major FDOM components, including the dominance of C1 at the upstream sites and C3 at the downstream sites  
257 and urban tributaries (Fig. S2). The differential EEMs obtained as the differences between the initial and final EEMs of the  
258 incubated samples showed site-specific contrasting patterns of DOM consumption (i.e., reduction in fluorescence intensity  
259 during the incubation; indicated by blue color on Fig. S2) around the region designated as C3 and DOM production (i.e.,  
260 increase in fluorescence intensity during the incubation; indicated by red color on Fig. S2) around C1 and C2 (Fig. S2). The  
261 differential EEMs of the forested headwater stream (Up 1) showed very little consumption or production compared to those  
262 for Up 2 and Up 3. While the differential EEMs of Mid 2 and Mid 3 were more pronounced in the production of new  
263 fluorescent components, all downstream samples revealed a predominant consumption to a greater extent than the upstream  
264 and midstream samples. The samples of Urban 1 also showed a predominance of consumption, but the two other urban  
265 tributaries displayed both consumption and production of DOM components.

### 266 3.2 Biodegradation and $\text{CO}_2$ production in the lower Han River and urban tributary

267 The concentration of BDOC ( $\text{mg C L}^{-1}$ ) measured during the 5 day incubation ranged from  $0.20 \text{ mg C L}^{-1}$  at the mainstem to



268 0.46 mg L<sup>-1</sup> at the urban tributary, with differences between the samples largely corresponding to the initial DOC  
269 concentrations (Fig. 5a). The BDOC concentrations of the mixture samples were similar to the expected average value of the  
270 samples incubated in isolation. However, the 5 day %BDOC values of all samples converged toward 10 %, with very small  
271 variations among the samples, after having passed a transition period between 24 and 72 h, when the mainstem samples  
272 showed the highest values (Fig. 5b). The dissolved CO<sub>2</sub> concentration was higher in the tributary sample than in the  
273 mainstem sample throughout the incubation (Fig. 5c). The dissolved CO<sub>2</sub> concentration in the mixture sample exceeded the  
274 conservative mixing average calculated from the CO<sub>2</sub> measurements of the two separate samples after the second day of  
275 incubation. Moreover, the cumulative CO<sub>2</sub> production in the mixture sample, which was calculated as the cumulative  
276 increase in dissolved CO<sub>2</sub> per unit water volume (mg C L<sup>-1</sup>), exceeded the rates found in the mainstem and tributary samples  
277 from the second day, with the average production rate higher than the conservative mixing average by 60 % (Fig. 5d).

278 The fluorescence EEMs of all initial samples prior to the incubation exhibited a predominance of the protein-like  
279 fluorescence peak around C3 (Fig. 6), contrasting with the EEM of the headwater stream sample dominated by the strong  
280 humic-like fluorescence peaks around C1 (Fig. S2). The fluorescence intensity of C3 was much higher in the tributary and  
281 mixture samples than in the mainstem samples (Fig. 6). The differential EEMs obtained as the differences between the initial  
282 and final EEMs for each incubation interval indicated a persistent consumption of protein-like components in the mainstem  
283 samples throughout the entire incubation period, as illustrated by blue color on the EEM indicating decreases in fluorescence  
284 intensity (Fig. 6). On the other hand, the production of new DOM components initially dominated the differential EEMs of  
285 the tributary samples, followed by the consumption of the newly produced components during the period from the first to  
286 the third day. The mixture samples showed more complex patterns with the consumption of protein-like components  
287 dominating during the first hour and a later phase from the first to the third day. Other optical properties of DOM also  
288 suggested a clear linkage between the consumption of protein-like components and DOM biodegradation (Fig. S3; Table S4).

289 Although fluorescence intensities of C3 and the other components were in the descending order of the tributary, mixture, and  
290 mainstem samples, the disproportionately large ratios among three fluorescent components and other fluorescence indices  
291 such as FI, HIX, and BIX observed for the mixture samples illustrate an overwhelming influence of the tributary OM on the  
292 optical signals of the mixture samples.

293 The FT-ICR mass spectra of the DOM extracted from the mainstem and tributary samples used in the second incubation  
294 experiment exhibited more than 4,000 peaks and widely scattered distributions of assigned molecular formulas on the van



295 Krevelen diagrams at both sites and wide (Fig. 7). When the results of the FT-ICR-MS analyses before and after the  
296 incubation were compared, the molecular formulas whose peak intensities increased or decreased during the incubation  
297 indicate the relative production or consumption of the corresponding DOM components, respectively, compared to the initial  
298 intensities. Consistent with the patterns observed for the differential EEMs (Fig. 6), the comparison of the pre- and post-  
299 incubation mainstem samples revealed more consumed organic molecules (3984 molecules) than the newly produced  
300 molecules (771 molecules). These patterns did not change when van Krevelen diagrams were produced with molecular  
301 formulas that showed 2-fold changes in peak intensity: 2303 consumed molecular formulas exceeding 601 produced  
302 molecular formulas (Fig. S4). In contrast, the tributary samples exhibited more production (2789 molecules) than  
303 consumption (1479 molecules) (Fig. 7). The production and consumption of molecular formulas were observed across the  
304 major molecular series including CHO, CHOP, CHOS, CHON, and CHONSP. At both sites the DOM composition was  
305 characterized by diverse molecular formulas enriched in heteroatoms (N, S, and P). Although no consistent pattern was  
306 evident for each of the major molecular series, the pronounced consumption in the mainstem sample was associated with the  
307 CHO and P-containing molecular formulas compared to the rather diffuse consumption pattern of the tributary sample.

## 308 4 Discussion

### 309 4.1 Longitudinal changes in optical properties and biodegradability of DOM

310 Downstream increases in BDOC and  $p\text{CO}_2$  along the Han River and its urban tributaries (Fig. 2) suggest that anthropogenic  
311 perturbations caused by water impoundment and pollution exert a strong influence on OM biodegradation in this highly  
312 modified river system. Deviations from the overall pattern of downstream increases in BDOC and  $p\text{CO}_2$ , as observed at  
313 some up-, mid-, and downstream sites (Fig. 2), might be explained by combined effects of local differences in the  
314 predominant land use, proximate pollution sources, and increased water retention along the impounded river reaches (Guo et  
315 al., 2014; Hosen et al., 2014; Hur et al., 2014a). For example, the increase in BDOC from Up 1 to Up 2 can be attributed to  
316 the intensive agricultural land use in the drained watershed (Jung et al., 2015). Streams draining agricultural lands have been  
317 shown to contain more bioavailable DOM moieties compared to forested and other natural streams (Bellmore et al., 2015;  
318 Petrone et al., 2011; Williams et al., 2010, 2016). The slightly higher BDOC concentrations ( $0.19 \pm 0.05 \text{ mg C}^{-1} \text{ L}^{-1}$ )  
319 and %BDOC ( $12.7 \pm 2.1 \%$ ) measured for the midstream reach than those for the upstream sites (Table S3a) might reflect  
320 the influence of labile autochthonous DOM components produced in the midstream reach that is impounded by a cascade of



321 dams ( Hur et al., 2014a; Williams et al., 2010). Highly variable BDOC concentrations at the downstream sites indicate the  
322 complex interplay between OM inputs from the upstream reservoirs and urban tributaries, the increased water retention by  
323 the weirs installed at both ends of the downstream reach, and tidal influences from the estuary (Guo et al., 2014; Hosen et al.,  
324 2014). Although urban tributaries bring high loads of bioavailable DOM to the downstream river (Fig. 2; Table S3),  
325 localized pulses of  $p\text{CO}_2$  along the confluences of the major urban tributaries observed in our continuous underway  
326 measurements of  $p\text{CO}_2$  along the same reach suggested rapid physical mixing and biological transformations of  $\text{CO}_2$  and  
327 OM in a relatively short section of the downstream river (Yoon et al., 2016). This localized effect of tributary inputs might  
328 explain the unexpectedly low BDOC concentration at Down 1 that is located downstream of the tributary Urban 2 (Fig. 2).

329 Similar to the high spatial variability observed for BDOC, optical properties were also highly variable across the mainstem  
330 and urban tributaries (Fig. 3; Fig. S1). Many optical properties exhibited positive relationships with BDOC concentrations  
331 (Fig. 4), as observed in other studies (Hosen et al., 2014; Knapik et al., 2015; Petrone et al., 2011; Williams et al., 2010).  
332 However,  $\text{SUVA}_{254}$  and HIX values were not correlated with BDOC concentrations. Very high values of  $\text{SUVA}_{254}$  and HIX  
333 found at the upstream sites compared to the downstream sites suggest a large contribution of terrestrial DOM components at  
334 the upstream sites and decreasing levels of humification along the downstream reaches (Helms et al., 2008). However, it is  
335 also possible that microbial production of humic-like DOM components can increase  $\text{SUVA}_{254}$  (Weishaar et al., 2003), as  
336 indicated by the slightly higher values of  $\text{SUVA}_{254}$  and HIX at the urban tributaries than at the downstream sites. The  
337 positive correlations between FI and BDOC concentrations imply a dominant contribution of autochthonous components to  
338 DOM biodegradation, consistent with previous findings (Petrone et al., 2011; Williams et al., 2010). Although all three  
339 FDOM components were correlated with BDOC concentrations, the regression slopes were steeper in the descending order  
340 of C3, C2, and C1 (Fig. 4), implying a greater contribution of protein-like FDOM components to BDOC. The strongly  
341 positive relationship between BDOC concentrations and in situ  $p\text{CO}_2$  measurements suggests that high loads of labile DOM  
342 components of autochthonous and allochthonous origin, such as protein-like FDOM components, can substantially enhance  
343 OM biodegradation in the eutrophic urban river, resulting in high rates of  $\text{CO}_2$  emission.

344 Spatial differences in the dominant FDOM components, i.e. C1 along the up- and midstream reaches vs. C3 along the  
345 downstream reach and urban tributaries (Fig. 3), illustrate a strong longitudinal alteration of DOM composition  
346 corresponding to the level of anthropogenic perturbation (Hosen et al., 2014). In addition to the downstream increase in  
347 protein-like fluorescence intensity, the increases in the ratios of C3/C1 and C3/C2 along the downstream reach highlight the



348 importance of the urban tributary input for DOM quality in urban rivers (Guo et al., 2014). The gradual downstream increase  
349 in FI in contrast to decreasing HIX also adds up to the downstream evolution of DOM quality, as often observed in other  
350 anthropogenically affected inland water systems (Hosen et al., 2014; Petrone et al., 2011; Williams et al., 2010, 2016). The  
351 higher BIX values in the downstream and urban tributary sites compared to the upstream sites can be explained by enhanced  
352 microbial activities in the urbanized reach. Other studies have also shown that DOM composition in the eutrophic urban  
353 river can be dominated by microbially produced components with characteristic blue-shifted fluorescence peaks (Lee et al.,  
354 2015; Parlanti et al., 2000; Williams et al., 2010, 2016).

355 The significant decreases in C3 peak intensity in the incubated downstream and urban tributary samples (Fig. S1a), along  
356 with pronounced microbial humic-like peaks on the fluorescence EEMs (Fig. S2), suggest that the consumption of labile  
357 DOM components might concur with the production of autochthonous DOM components. In addition, the decrease in the  
358 ratio of C3:C1 and C3:C2 (Fig. S1a) indicates a preferential consumption of protein-like components. The 7 day incubation  
359 with and without particulates did not show significant differences in BDOC concentration and other optical properties at all  
360 sites, probably due to the relatively low concentrations of TSS in the water samples collected during the dry season (Table  
361 S3b). If the incubation were conducted with samples collected during high-flow periods that would have much higher TSS  
362 and POM concentrations, the contribution of particulates to BDOC might be more evident across the sites (Jung et al., 2015).

363 Future research should encompass more diverse urban water systems including pollution sources such as WWTP effluents  
364 and seasonal variability in hydrologic conditions to better constrain the spatial and temporal patterns of DOM properties and  
365 biodegradation in anthropogenically modified river systems.

#### 366 **4.2 Priming effects of urban tributary inputs on riverine biodegradation and CO<sub>2</sub> production**

367 The unexpectedly high rate of cumulative CO<sub>2</sub> production in the mixture sample exceeding the rates measured for the  
368 separate samples (Fig. 5d) supports our hypothesis that the mixing of the mainstem and urban tributary waters can enhance  
369 the biodegradation of “native” stable organic components in the presence of “external” labile materials, consistent with  
370 positive priming effects observed in various aquatic systems (Bianchi et al., 2015; Guenet et al., 2014; Hotchkiss et al.,  
371 2014; Kuehn et al., 2014). Inputs of external labile organic materials can provide heterotrophic microbial decomposers with  
372 energy-rich compounds, promoting the overall metabolic capacity through increases in microbial cells and/or the activity of  
373 enzymes involved in degrading recalcitrant components (Guenet et al., 2014; Hotchkiss et al., 2014; Kuehn et al., 2014).



374 Although labile organic moieties in algal and macrophyte exudates have been shown to prime the biodegradation of  
375 allochthonous organic materials in artificially concocted water samples, few studies have examined how microbial  
376 organisms would respond to the addition of labile compounds to the existing organic materials in real river waters with  
377 different levels of OM lability (Hotchkiss et al., 2014; Kuehn et al., 2014). Identifying sources and target components of  
378 priming is very challenging because our experimental design did not include model compounds with distinct chemical  
379 signatures such as C isotopes that could be used to track priming-induced changes in optical properties of different DOM  
380 components (Bianchi et al., 2015). However, the increased rate of CO<sub>2</sub> production and more complex changes in the  
381 fluorescence EEMs of the mixture samples provided indirect lines of evidence for the enhanced degradation of stable OM  
382 moieties in the presence of more labile components that might have been produced in the upstream reservoirs or during the  
383 transport along the downstream reach receiving polluted urban streams.

384 More complex patterns of the EEM peaks observed for the mixture samples than those for the separate samples (Fig. 6)  
385 provide a visual manifestation of priming-enhanced alterations of DOM composition. The pronounced enhancement  
386 (“production”) and subsequent decrease (“consumption”) in the intensity of fluorescence peaks around C2 over the first  
387 three days indicate a significant contribution of microbially produced or converted materials to the overall microbial  
388 processing of the OM pool becoming increasingly depleted of labile components. The prevailing consumption of labile  
389 DOM components in the mainstem samples, as indicated by the differential EEMs dominated by the reduction of the  
390 protein-like fluorescence (C3), agrees with the decreased peak intensities of as many as 3984 molecular formulas identified  
391 by the FT-ICR-MS analysis (Fig. 7). The alternation of the strong enhancement and reduction of two humic-like FDOM  
392 components (C1 and C2) shown on the tributary differential EEMs, combined with the produced molecular formulas (2789  
393 peaks) exceeding the consumed molecular formulas (1479 peaks) on the van Krevelen diagrams, supports the idea of active  
394 processing of the tributary DOM pool, which might have been accelerated further following the addition of more labile  
395 components contained in the mainstem to the tributary water.

396 The van Krevelen diagrams of both mainstem and tributary samples exhibited a large number of organic molecules with  
397 molecular formula distributions similar to those found for anthropogenically impacted rivers (Arnold et al., 2014; Gonsior et  
398 al., 2011; Mesfioui et al., 2012; Wagner et al., 2015). The observed complex patterns of molecular formula distribution are  
399 distinguished from the molecular formulas identified for unaffected headwater streams, which are usually dominated by  
400 CHO molecular series and lignin-like components characterized by an O/C molar ratio of 0.25–0.5 and an H/C molar ratio



401 of 1–1.5 (Jaffé et al., 2012; Kim et al., 2006; Lu et al., 2015). It has been shown that the composition of DOM in natural  
402 waters is dominated by C, H, O, and N, with minor contributions of P and S (Koch et al., 2007). While comparing molecular  
403 signatures identified for ten global rivers, Wagner et al. (2015) found the molecular formulas unique to anthropogenically  
404 impacted rivers, including highly diverse heteroatomic formulas enriched in N and S, which have also been identified in  
405 wastewater effluents and septic waters (Arnold et al., 2014; Gonsior et al., 2011; Mesfioui et al., 2012). Compared to the  
406 usual composition of molecular series identified for headwater streams (Lu et al., 2015) and large rivers with low levels of  
407 pollution (Wagner et al., 2015), the high enrichment of N- and S-containing formulas in both the mainstem and tributary  
408 samples (Figs. 7, S4) points to the strong influence of anthropogenic DOM across the downstream reaches and urban  
409 tributaries. The high enrichment of S-containing formulas in WWTP effluents has been attributed to the presence of  
410 surfactants and their co-products and biodegraded metabolites (Gonsior et al., 2011). Incubation-induced decreases of CHOP  
411 and CHONSP formulas in the range of the O/C molar ratio of 0–0.2 and an H/C molar ratio of 0.5–1, which has been  
412 associated with condensed hydrocarbons, were particularly distinct on the “consumption” diagram of the mainstem sample,  
413 indicating a preferential consumption of labile, P-containing components that might have been transferred from the upstream  
414 reservoir and/or produced in the slowly moving water along the mainstem channel. Other studies have also shown that the  
415 van Krevelen diagrams of the DOM dominated by materials produced in lakes or impounded rivers are characterized by  
416 condensed hydrocarbon regions and higher proportions of heteroatomic formulas containing N, S, and P (Minor et al., 2012;  
417 Wagner et al., 2015).

418 Previous incubation studies employing FT-ICR-MS showed a biodegradation-induced shift in mass distribution toward a  
419 dominance of lower-mass molecules (Kim et al., 2006) and a rather selective consumption of bioreactive molecules  
420 associated with protein- and lipid-like regions of the van Krevelen diagrams (Lu et al., 2015). Unlike the preferential  
421 utilization of higher molecular weight fraction observed in upstream streams (Kim et al., 2006), a wide range of produced or  
422 consumed molecular formulas identified on the van Krevelen diagrams (Figs. 7, S4) might indicate a high potential of  
423 microbial processing of organic molecules in both mainstem and tributary samples. However, the greater number of newly  
424 produced molecules relative to the small number of consumed molecules in the tributary samples, combined with mixing-  
425 enhanced changes in CO<sub>2</sub> production and optical indices, suggests that organic materials in the urban tributary are already  
426 highly processed by microbial decomposers that might be limited by labile components, unlike the mainstem water that  
427 appears to contain more labile, autochthonous materials derived from the upstream impounded reach.



428 The prevailing OM consumption observed in the mainstem samples is consistent with the fact that decreases in both  
429 fluorescence ratios C3/C1 and C3/C2 were steeper in the mainstem than in the tributary samples (Fig. S3). The preferential  
430 consumption of protein-like components relative to more recalcitrant components implies the relative abundance of  
431 bioreactive molecules in the mainstem samples receiving high inputs of labile autochthonous DOM produced in the  
432 upstream reservoirs, as often observed in other impounded rivers (Hur et al., 2014a; Stanley et al., 2011). In the case of the  
433 tributary DOM dynamics, the production of DOM components was pronounced during the initial phase, indicating rapid  
434 production and/or transformation from depleting bioavailable DOM components including the labile fraction of POM.  
435 Another possible explanation for the high OM production in the tributary sample might be substrate-specific high efficiency  
436 of microbial assimilation of highly processed DOM components in the tributary (Ward et al., 2013). Eutrophic urban streams  
437 and rivers receiving untreated or treated wastewaters have been found to contain characteristic microbial communities,  
438 which are often less diverse but highly efficient in utilizing food resources available in the urban water environment than in  
439 less affected waters (Shanks et al., 2013; Winter et al., 2007). The diversification of C sources in the mixture samples was  
440 likely to prime the degradation of stable organic components in both source waters (Kuehn et al., 2014). The processing of  
441 OM in the mixture samples might have been accelerated by the addition of a microbial community that is efficient in  
442 assimilating organic compounds available in the urban tributary to the mainstem sample enriched in labile DOM  
443 components, as illustrated by complex patterns of EEM peaks switching toward a pattern dominated by consumption (Fig.  
444 6) that concurred with the increasing rate of CO<sub>2</sub> production (Fig. 5).

445 Complementing the conventional approach based on BDOC determination with continuous measurements of dissolved CO<sub>2</sub>  
446 in unfiltered water samples provided data supporting the contribution of labile particulate components to DOM  
447 biodegradation and CO<sub>2</sub> production in the eutrophic river. The greater production of CO<sub>2</sub> than what we could expect from  
448 the cumulative BDOC during the 5 day incubation (Fig. 5a, 5d) implies a significant contribution of the soluble fraction of  
449 POM to the C mineralization particularly in the mixture sample. Despite a number of recent efforts to examine  
450 anthropogenic perturbations to riverine carbon dynamics, only a small number of studies have explicitly addressed the  
451 conversion between DOM and POM components (Jung et al., 2015; Osburn et al., 2012) and fewer studies have measured  
452 BDOC and CO<sub>2</sub> production simultaneously. When the biodegradability and optical properties of POM-derived labile  
453 components were compared with those for DOM in different types of inland waters, unique fluorescence signatures found  
454 for DOM components leached from particulates became more pronounced over the course of incubation and the origin of



455 these components was often ascribed to enhanced microbial processing of OM in eutrophic waters (Jung et al., 2015; Osburn  
456 et al., 2012). Quantifying the contribution of the labile fraction of POM to DOM biodegradation would be very difficult due  
457 to the continuous conversion between POM and DOM during downstream transport (del Giorgio and Pace, 2008; Jung et al.,  
458 2015).

## 459 **5 Conclusions**

460 Complex longitudinal patterns of  $p\text{CO}_2$  and the optical properties and biodegradability of DOM observed in the Han River  
461 suggest that the traditional view of gradual downstream changes in riverine OM composition based on the river continuum  
462 concept (Vannote et al., 1980) may be invalid in explaining discontinuities in DOM properties and biodegradability across  
463 the impounded or polluted river reaches of highly modified river systems. Although the limited sampling frequency and  
464 spatial coverage did not allow us to examine local land use effects at high spatial and temporal resolutions, the field survey  
465 combining in situ  $p\text{CO}_2$  measurements and laboratory incubations revealed two pronounced longitudinal patterns reflecting  
466 the dominant anthropogenic perturbations to the studied river system: impoundment effects along the midstream reach and  
467 water pollution effects along the downstream reach. Increased primary production in the impounded reach, as indicated by  
468 lower  $p\text{CO}_2$  values as compared with the upstream reach, can enhance the biodegradability of DOM by providing labile  
469 DOM components of autochthonous origin. The downstream reach receiving the dam discharge enriched in autochthonous  
470 organic materials and urban tributaries delivering anthropogenic materials discharged from WWTPs exhibited substantially  
471 elevated levels of  $p\text{CO}_2$  and DOM optical indices. However, large spatial variabilities in  $p\text{CO}_2$  and BDOC across the  
472 downstream sites and urban tributaries suggest that microbial OM processing in the mixed waters from the upstream  
473 reservoir and urban tributaries can occur very rapidly along short river sections receiving urban tributaries and at paces that  
474 have not been observed in natural river systems.

475 Unlike the recent studies of priming effects on DOM biodegradation that have focused on the stimulation of the  
476 biodegradation of the recalcitrant terrestrial DOM by labile autochthonous components (Bianchi et al., 2015; Catalan et al.,  
477 2015; Hotchkiss et al., 2014; Kuehn et al., 2014), the mixing-induced changes in  $\text{CO}_2$  production and DOM optical  
478 properties in the second incubation experiment, which were distinctively larger than the values measured separately in the  
479 urban tributary and the river water receiving dam discharge, underscore the importance of microbial processing in  
480 transforming OM components of both autochthonous and anthropogenic origin and subsequently inducing a priming effect



481 on the biodegradation of the bulk riverine OM in the eutrophic streams and rivers draining highly modified river systems.  
482 The larger rate of CO<sub>2</sub> production than the BDOC measured in the unfiltered mixture sample pointed to the potential  
483 contribution of POM, raising a possibility that the conventional experimental design excluding the particulate component  
484 might significantly underestimate priming effects on the biodegradation of the actual riverine OM that includes both DOM  
485 and POM. Considering that under real field conditions photodegradation can accelerate the biodegradation of physically  
486 degraded OM components, priming effects may be stronger in the field than in the dark incubator. Therefore, future research  
487 should involve in situ measurements of OM biodegradation and CO<sub>2</sub> production by conducting incubation experiments  
488 under both dark and light conditions. If isotopically distinct or labelled materials are used in field incubation experiments,  
489 the results can also be used to track the sources of the released CO<sub>2</sub> and the pathways of OM conversion. To better assess the  
490 role of anthropogenically impacted rivers in the regional and global carbon budgets, more field-based studies of site-specific  
491 anthropogenic influences should be conducted in a wide range of systems including urban, agricultural, and impounded  
492 rivers.

#### 493 **Data availability**

494 Data are available and can be requested from the corresponding author (jhp@ewha.ac.kr).

#### 495 **Supporting information**

496 Materials and Methods described in detail, supplementary tables (Table S1; Table S2; Table S3a; Table S3b; Table S4a;  
497 Table S4b) and supplementary figures (Fig. S1a; Fig. S1b; Fig. S2; Fig. S3).

#### 498 **Author contribution**

499 All authors contributed to data acquisition, the discussion of the results, and manuscript preparation. The manuscript was  
500 written by concerted efforts of J.-H. Park, H. B. Oh, and M.S. Begum.

#### 501 **Competing interests**

502 The authors declare that they have no conflict of interest.

#### 503 **Acknowledgments**

504 This work was supported by the National Research Foundation of Korea funded by the Korean Government  
505 (2014R1A2A2A01006577). We thank Dr. Tae Kyung Yoon and Borami Park for their assistance with sampling and analysis.



506 References

- 507 Abril, G., Nogueira, M., Etcheber, H., Cabeçadas, G., Lemaire, E. and Brogueira, M.: Behaviour of organic carbon in nine  
508 contrasting European estuaries, *Estuar. Coast. Shelf Sci.*, 54, 241–262, doi:10.1006/ecss.2001.0844, 2002.
- 509 Arnold, W. A., Longnecker, K., Kroeger, K. D. and Kujawinski, E. B., Molecular signature of organic nitrogen in septic-  
510 impacted groundwater, *Environ. Sci. Process. Impacts*, 16 (10), 2400–2407, 2014.
- 511 Aufdenkampe, A. K., Mayorga, E., Raymond, P. A., Melack, J. M., Doney, S. C., Alin, S. R., Aalto, R. E. and Yoo, K.:  
512 Riverine coupling of biogeochemical cycles between land, oceans, and atmosphere, *Front. Ecol. Environ.*, 9(1), 53–60,  
513 doi:10.1890/100014, 2011.
- 514 Baker, A.: Fluorescence excitation-emission matrix characterization of some sewage-impacted rivers, *Environ. Sci. Technol.*,  
515 35(5), 948–953, doi:10.1021/es000177t, 2001.
- 516 Bastviken, D., Tranvik, L. J., Downing, J. A., Crill, P. M., and Enrich-Prast, A.: Freshwater methane emissions offset the  
517 continental carbon sink, *Science*, 331, 50, 2011.
- 518 Bellmore, R., Harrison, J., Needoba, J., Brooks, E. and Keller, C.: Hydrologic control of dissolved organic matter  
519 concentration and quality in a semiarid artificially drained agricultural catchment, *Water Resour. Res.*, 51, 8146–8164,  
520 doi:10.1002/2015WR016884, 2015.
- 521 Bianchi, T. S.: The role of terrestrially derived organic carbon in the coastal ocean: A changing paradigm and the priming  
522 effect, *Proc. Natl. Acad. Sci.*, 108(49), 19473–19481, doi:10.1073/pnas.1017982108, 2011.
- 523 Bianchi, T. S., Thornton, D. C. O., Yvon-lewis, S. A., King, G. M., Eglinton, T. I., Shields, M. R., Ward, N. D. and Curtis, J.:  
524 Organic matter in a freshwater microcosm system, *Geophys. Resesarch Lett.*, 42, 5460–5467, doi:10.1002/  
525 2015GL064765, 2015.
- 526 Casas-Ruiz, J. P., Tittel, J., von Schiller, D., Catalán, N., Obrador, B., Gómez-Gener, L., Zwirnmann, E., Sabater, S. and  
527 Marcé, R.: Drought-induced discontinuities in the source and degradation of dissolved organic matter in a Mediterranean  
528 river, *Biogeochemistry*, 127, 125–139, doi:10.1007/s10533-015-0173-5, 2016.
- 529 Catalan, N., Kellerman, A. M., Peter, H., Carmona, F. and Tranvik, L. J.: Absence of a priming effect on dissolved organic  
530 carbon degradation in lake water, *Limnol. Oceanogr.*, 60, 159–168, doi:10.1002/lno.10016, 2015.
- 531 Chang, H.: Spatial analysis of water quality trends in the Han River basin, South Korea, *Water Res.*, 42, 3285–3304,  
532 doi:10.1016/j.watres.2008.04.006, 2008.



- 533 Cole, J. J., Prairie, Y. T., Caraco, N. F., McDowell, W. H., Tranvik, L. J., Striegl, R. G., Duarte, C. M., Kortelainen, P.,  
534 Downing, J. A., Middelburg, J. J. and Melack, J.: Plumbing the global carbon cycle: Integrating inland waters into the  
535 terrestrial carbon budget, *Ecosystems*, 10(1), 171–184, doi:10.1007/s10021-006-9013-8, 2007.
- 536 Dittmar, T., Koch, B., Hertkorn, N. and Kattner, G.: A simple and efficient method for the solid-phase extraction of dissolved  
537 organic matter (SPE-DOM) from seawater, *Limnol. Ocean. Methods*, 6, 230–235, doi:10.4319/lom.2008.6.230, 2008.
- 538 Fellman, J. B., Hood, E. and Spencer, R. G. M.: Fluorescence spectroscopy opens new windows into dissolved organic  
539 matter dynamics in freshwater ecosystems: A review, *Limnol. Oceanogr.*, 55(6), 2452–2462,  
540 doi:10.4319/lo.2010.55.6.2452, 2010.
- 541 del Giorgio, P. a. and Pace, M. L.: Relative independence of dissolved organic carbon transport and processing in a large  
542 temperate river: The Hudson River as both pipe and reactor, *Limnol. Oceanogr.*, 53(1), 185–197,  
543 doi:10.4319/lo.2008.53.1.0185, 2008.
- 544 Gonsior, M., Zwartjes, M., Cooper, W. J., Song, W., Ishida, K.P., Tseng, L. Y., Jeung, M. K., Rosso, D., Hertkorn, N., and  
545 Schmitt-Kopplin, P.: Molecular characterization of effluent organic matter identified by ultrahigh resolution mass  
546 spectrometry, *Water Res.*, 45, 2943–2953, 2011.
- 547 Guenet, B., Danger, M., Harrault, L., Allard, B., Jauset-Alcala, M., Bardoux, G., Benest, D., Abbadie, L. and Lacroix, G.:  
548 Fast mineralization of land-born C in inland waters: First experimental evidences of aquatic priming effect, *Hydrobiologia*,  
549 721(1), 35–44, doi:10.1007/s10750-013-1635-1, 2014.
- 550 Guo, W., Yang, L., Zhai, W., Chen, W., Osburn, C. L., Huang, X. and Li, Y.: Runoff-mediated seasonal oscillation in the  
551 dynamics of dissolved organic matter in different branches of a large bifurcated estuary - The Changjiang Estuary, *J.*  
552 *Geophys. Res. Biogeosciences*, 119(5), 776–793, doi:10.1002/2013JG002540, 2014.
- 553 Helms, J. R., Stubbins, A., Ritchie, J. D., Minor, E. C., Kieber, D. J. and Mopper, K.: Absorption spectral slopes and slope  
554 ratios as indicators of molecular weight, source, and photobleaching of chromophoric dissolved organic matter,  
555 *Limnology Oceanogr.*, 53(3), 955–969, doi:10.4319/lo.2008.53.3.0955, 2008.
- 556 Hosen, J. D., McDonough, O. T., Febria, C. M. and Palmer, M. A.: Dissolved organic matter quality and bioavailability  
557 changes across an urbanization gradient in headwater streams, *Environ. Sci. Technol.*, 48(14), 7817–7824,  
558 doi:10.1021/es501422z, 2014.
- 559 Hotchkiss, E. R., Hall, R. O., Baker, M. A., Rosi-Marshall, E. J. and Tank, J. L.: Modeling priming effects on microbial



- 560 consumption of dissolved organic carbon in rivers, *J. Geophys. Res. Biogeosciences*, 119(5), 982–995,  
561 doi:10.1002/2013JG002599, 2014.
- 562 Huguet, A., Vacher, L., Relexans, S., Saubusse, S., Froidefond, J. M. and Parlanti, E.: Properties of fluorescent dissolved  
563 organic matter in the Gironde Estuary, *Org. Geochem.*, 40(6), 706–719, doi:10.1016/j.orggeochem.2009.03.002, 2009.
- 564 Hur, J., Lee, B.-M., Lee, S. and Shin, J.-K.: Characterization of chromophoric dissolved organic matter and trihalomethane  
565 formation potential in a recently constructed reservoir and the surrounding areas - Impoundment effects, *J. Hydrol.*, 515,  
566 71–80, doi:10.1016/j.jhydrol.2014.04.035, 2014a.
- 567 Hur, J., Nguyen, H. V. M. and Lee, B. M.: Influence of upstream land use on dissolved organic matter and trihalomethane  
568 formation potential in watersheds for two different seasons, *Environ. Sci. Pollut. Res.*, 21(12), 7489–7500,  
569 doi:10.1007/s11356-014-2667-4, 2014b.
- 570 Hutrya, L. R., Duren, R., Gurney, K. R., Grimm, N., Kort, E. a., Larson, E. and Shrestha, G.: Urbanization and the carbon  
571 cycle: Current capabilities and research outlook from the natural sciences perspective, *Earth's Futur.*, 2(10), 473–495,  
572 doi:10.1002/2014EF000255, 2014.
- 573 Jaffé, R., Yamashita, Y., Maie, N., Cooper, W. T., Dittmar, T., Dodds, W. K., Jones, J. B., Myoshi, T., Ortiz-Zayas, J. R.,  
574 Podgorski, D. C. and Watanabe, A.: Dissolved organic matter in headwater streams: Compositional variability across  
575 climatic regions of North America, *Geochim. Cosmochim. Acta*, 94, 95–108, doi:10.1016/j.gca.2012.06.031, 2012.
- 576 Johnson, M., Billett, M., Dinsmore, K., Wallin, M., Dyson, K. and Jassal, R.: Direct and continuous measurement of  
577 dissolved carbon dioxide in freshwater aquatic systems – Method and applications, *Ecohydrology*, 3, 68–78,  
578 doi:10.1002/eco.95, 2010.
- 579 Jung, B. J., Jeanneau, L., Alewell, C., Kim, B. and Park, J. H.: Downstream alteration of the composition and  
580 biodegradability of particulate organic carbon in a mountainous, mixed land-use watershed, *Biogeochemistry*, 122(1), 79–  
581 99, doi:10.1007/s10533-014-0032-9, 2015.
- 582 Jung, S. W., Kwon, O. Y., Yun, S. M., Joo, H. M., Kang, J.-H. and Lee, J. H.: Impacts of dam discharge on river  
583 environments and phytoplankton communities in a regulated river system, the lower Han River of South Korea, *J. Ecol.*  
584 *Environ.*, 37(1), 1–11, doi:10.5141/ecoenv.2014.001, 2014.
- 585 Kang, M. G. and Park, S. W.: An adaptive watershed management assessment based on watershed investigation data, *Environ.*  
586 *Manage.*, 55(5), 1006–1021, doi:10.1007/s00267-014-0442-4, 2015.



- 587 Kaushal, S. S., McDowell, W. H. and Wollheim, W. M.: Tracking evolution of urban biogeochemical cycles: past, present,  
588 and future, *Biogeochemistry*, 121(1), 1–21, doi:10.1007/s10533-014-0014-y, 2014.
- 589 Kim, S., Kaplan, L. A. and Hatcher, P. G.: Biodegradable dissolved organic matter in a temperate and a tropical stream  
590 determined from ultra-high resolution mass spectrometry, *Limnol. Oceanogr.*, 51(2), 1054–1063,  
591 doi:10.4319/lo.2006.51.2.1054, 2006.
- 592 Knapik, H. G., Fernandes, C. V. S., de Azevedo, J. C. R., dos Santos, M. M., Dall’Agnol, P. and Fontane, D. G.:  
593 Biodegradability of anthropogenic organic matter in polluted rivers using fluorescence, UV, and BDOC measurements,  
594 *Environ. Monit. Assess.*, 187(3), 104, doi:10.1007/s10661-015-4266-3, 2015.
- 595 Koch, B. P., Dittmar, T., Witt, M. and Kattner, G.: Fundamentals of molecular formula assignment to ultrahigh resolution  
596 mass data of natural organic matter, *Anal. Chem.*, 79(4), 1758–1763, doi:10.1021/AC061949S, 2007.
- 597 Kuehn, K. A., Francoeur, S. N., Findlay, R. H. and Neely, R. K.: Priming in the microbial landscape: Periphytic algal  
598 stimulation of litter-associated microbial decomposers, *Ecology*, 95(3), 749–762, doi:10.1890/13-0430.1, 2014.
- 599 Kuzyakov, Y., Friedel, J. K. and Stahr, K.: Review of mechanisms and quantification of priming effects, *Soil Biol. Biochem.*,  
600 32, 1485–1498, doi:10.1016/S0038-0717(00)00084-5, 2000.
- 601 Lee, S. T., Yang, B., Kim, J.-Y., Park, J.-H. and Moon, M. H.: Combining asymmetrical flow field-flow fractionation with  
602 on- and off-line fluorescence detection to examine biodegradation of riverine dissolved and particulate organic matter, *J.*  
603 *Chromatogr. A*, 1409, 218–225, doi:10.1016/j.chroma.2015.07.074, 2015.
- 604 Lu, Y., Li, X., Mesfoui, R., Bauer, J. E., Chambers, R. M., Canuel, E. A. and Hatcher, P. G.: Use of ESI-FTICR-MS to  
605 characterize dissolved organic matter in headwater streams draining forest-dominated and pasture-dominated watersheds,  
606 *PLoS One*, 10(12), 1–21, doi:10.1371/journal.pone.0145639, 2015.
- 607 McElmurry, S. P., Long, D. T. and Voice, T. C.: Stormwater dissolved organic matter: influence of land cover and  
608 environmental factors, *Environ. Sci. Technol.*, 48(1), 45–53, doi:10.1021/es402664t, 2014.
- 609 McKnight, D. M., Boyer, E. W., Westerhoff, P. K., Doran, P. T., Kulbe, T. and Anderson, D. T.: Spectrofluorometric  
610 characterization of dissolved organic matter for indication of precursor organic material and aromaticity, *Limnol.*  
611 *Oceanogr.*, 46(1), 38–48, doi:10.4319/lo.2001.46.1.0038, 2001.
- 612 McLafferty, F., and Turecek, F.: *Interpretation of Mass Spectra*, 4th ed., University Science Books, Sausalito, California.,  
613 1993.



- 614 Minor, E. C., Steinbring, C. J., Longnecker, K. and Kujawinski, E. B.: Characterization of dissolved organic matter in Lake  
615 Superior and its watershed using ultrahigh resolution mass spectrometry, *Org. Geochem.*, 43, 1–11, 2012.
- 616 Ministry of Environment Korea: <https://www.me.go.kr/hg/web/index.do?menuId=998>, last access: 27 February 2017
- 617 Ministry of Land, Infrastructure, and Transport (MOLIT) Korea: [http://www.hrfco.go.kr/eng/service\\_1.do](http://www.hrfco.go.kr/eng/service_1.do), last access: 27  
618 February 2017, 2006.
- 619 Ohno, T.: Fluorescence inner-filtering correction for determining the humification index of dissolved organic matter, *Environ.*  
620 *Sci. Technol.*, 36(4), 742–746, doi:10.1021/es0155276, 2002.
- 621 Osburn, C. L., Handsel, L. T., Mikan, M. P., Paerl, H. W. and Montgomery, M. T.: Fluorescence tracking of dissolved and  
622 particulate organic matter quality in a river-dominated estuary, *Environ. Sci. Technol.*, 46(16), 8628–8636,  
623 doi:10.1021/es3007723, 2012.
- 624 Parlanti, E., Worz, K., Geoffroy, L. and Lamotte, M.: Dissolved organic matter fluorescence spectroscopy as a tool to  
625 estimate biological activity in a coastal zone submitted to anthropogenic inputs, *Org. Geochem.*, 31, 1765–1781,  
626 doi:10.1016/S0146-6380(00)00124-8, 2000.
- 627 Parr, T. B., Cronan, C. S., Ohno, T., Findlay, S. E. G., Smith, S. M. C. and Simon, K. S.: Urbanization changes the  
628 composition and bioavailability of dissolved organic matter in headwater streams, *Limnol. Oceanogr.*, 60(3), 885–900,  
629 doi:10.1002/lno.10060, 2015.
- 630 Petrone, K. C., Fellman, J. B., Hood, E., Donn, M. J. and Grierson, P. F.: The origin and function of dissolved organic matter  
631 in agro-urban coastal streams, *J. Geophys. Res. Biogeosciences*, 116(1), G01028, doi:10.1029/2010JG001537, 2011.
- 632 R Development Core Team: R: A language and environment for statistical computing; R Foundation for Statistical  
633 Computing: Vienna, Austria, available at <https://www.r-project.org>: last access 27 February 2017.
- 634 Raymond, P. a, Hartmann, J., Lauerwald, R., Sobek, S., McDonald, C., Hoover, M., Butman, D., Striegl, R., Mayorga, E.,  
635 Humborg, C., Kortelainen, P., Durr, H., Meybeck, M., Ciais, P. and Guth, P.: Global carbon dioxide emissions from inland  
636 waters, *Nature*, 503(7476), 355–359, doi:10.1038/nature12760, 2013.
- 637 Regnier, P., Friedlingstein, P., Ciais, P., Mackenzie, F. T., Gruber, N., Janssens, I. a., Laruelle, G. G., Lauerwald, R., Luyssaert,  
638 S., Andersson, A. J., Arndt, S., Arnosti, C., Borges, A. V., Dale, A. W., Gallego-Sala, A., Godd eris, Y., Goossens, N.,  
639 Hartmann, J., Heinze, C., Ilyina, T., Joos, F., LaRowe, D. E., Leifeld, J., Meysman, F. J. R., Munhoven, G., Raymond, P. A.,  
640 Spahni, R., Suntharalingam, P. and Thullner, M.: Anthropogenic perturbation of the carbon fluxes from land to ocean, *Nat.*



- 641 Geosci., 6(8), 597–607, doi:10.1038/ngeo1830, 2013.
- 642 Royer, T. V. and David, M. B.: Export of dissolved organic carbon from agricultural streams in Illinois, USA, *Aquat. Sci.*,  
643 67(4), 465–471, doi:10.1007/s00027-005-0781-6, 2005.
- 644 Servais, P., Billen, G. and Hascoet, M.-C.: Determination of the biodegradable fraction of dissolved organic matter in waters,  
645 *Water Res.*, 21(4), 445–450, doi:10.1016/0043-1354(87)90192-8, 1987.
- 646 Shanks, O. C., Newton, R. J., Kelty, C. A., Huse, S. M., Sogin, M. L. and McLellan, S. L.: Comparison of the microbial  
647 community structures of untreated wastewaters from different geographic locales, *Appl. Environ. Microbiol.*, 79(9), 2906–  
648 2913, doi:10.1128/AEM.03448-12, 2013.
- 649 Shi, J., Cui, H., Jia, L., Qiu, L., Zhao, Y., Wei, Z., Wu, J. and Wen, X.: Bioavailability of riverine dissolved organic carbon  
650 and nitrogen in the Heilongjiang watershed of northeastern China, *Environ. Monit. Assess.*, 188(2), 113,  
651 doi:10.1007/s10661-016-5120-y, 2016.
- 652 Spencer, R. G. M., Butler, K. D. and Aiken, G. R.: Dissolved organic carbon and chromophoric dissolved organic matter  
653 properties of rivers in the USA, *J. Geophys. Res. Biogeosciences*, 117(3), G03001, doi:10.1029/2011JG001928, 2012.
- 654 Stanley, E. H., Powers, S. M., Lottig, N. R., Buffam, I. and Crawford, J. T.: Contemporary changes in dissolved organic  
655 carbon (DOC) in human-dominated rivers: Is there a role for DOC management?, *Freshw. Biol.*, 57, 26–42,  
656 doi:10.1111/j.1365-2427.2011.02613.x, 2011.
- 657 Stubbins, A., Spencer, R.G.M., Chen, H., Hatcher, P.G., Mopper, K., Hernes, P.J., Mwamba, V.L., Mangangu, A. M.,  
658 Wabakanghanzi, J.N., Six, J.: Illuminated darkness: molecular signature of Congo river dissolved organic matter and its  
659 photochemical alteration as revealed by ultrahigh precision mass spectrometry, *Limnol. Oceanogr.*, 55(4), 1467–1477,  
660 DOI: 10.4319/lo.2010.55.4.1467, 2010.
- 661 Vannote, R.L., Minshall, G.W., Cummins, K.W., Sedell, J.R., Cushing, C.E.: The river continuum concept, *Can. J. Fish.*  
662 *Aquat. Sci.*, 37, 130–137, 1980.
- 663 Wagner, S., Riedel, T., Niggemann, J., Vähätalo, A. V., Dittmar, T. and Jaffé, R.: Linking the molecular signature of  
664 heteroatomic dissolved organic matter to watershed characteristics in world rivers, *Environ. Sci. Technol.*, 49(23), 13798–  
665 13806, doi:10.1021/acs.est.5b00525, 2015.
- 666 Ward, N. D., Keil, R. G., Medeiros, P. M., Brito, D. C., Cunha, A. C., Dittmar, T., Yager, P. L., Krusche, A. V. and Richey, J.  
667 E.: Degradation of terrestrially derived macromolecules in the Amazon River, *Nat. Geosci.*, 6(7), 530–533,



- 668 doi:10.1038/ngeo1817, 2013.
- 669 Water Resources Management Information System (WAMIS): [http://www.wamis.go.kr/ENG/WKB\\_LCSTBB\\_LST.aspx](http://www.wamis.go.kr/ENG/WKB_LCSTBB_LST.aspx),  
670 last access: 27 February 2017.
- 671 Wehrli, B.: Conduits of the carbon cycle, *Nature*, 503(21), 346–347, doi:10.1038/503346a, 2013.
- 672 Weishaar, J. L., Aiken, G. R., Bergamaschi, B. A., Fram, M. S., Fujii, R. and Mopper, K.: Evaluation of specific ultra-violet  
673 absorbance as an indicator of the chemical composition and reactivity of dissolved organic carbon, *Environ. Sci. Technol.*,  
674 37(20), 4702–4708, doi:10.1021/es030360x, 2003.
- 675 Wickland, K. P., Aiken, G. R., Butler, K., Dornblaser, M. M., Spencer, R. G. M. and Striegl, R. G.: Biodegradability of  
676 dissolved organic carbon in the Yukon River and its tributaries: Seasonality and importance of inorganic nitrogen, *Global  
677 Biogeochem. Cycles*, 26(3), GB0E03, doi:10.1029/2012GB004342, 2012.
- 678 Williams, C. J., Yamashita, Y., Wilson, H. F., Jaffe, R., Xenopoulos, M. a., Jaffé, R. and Xenopoulos, M. a.: Unraveling the  
679 role of land use and microbial activity in shaping dissolved organic matter characteristics in stream ecosystems, *Limnol.  
680 Oceanogr.*, 55(3), 1159–1171, doi:10.4319/lo.2010.55.3.1159, 2010.
- 681 Williams, C. J., Frost, P. C., Morales-Williams, A. M., Larson, J. H., Richardson, W. B., Chiandet, A. S. and Xenopoulos, M.  
682 A.: Human activities cause distinct dissolved organic matter composition across freshwater ecosystems, *Glob. Chang.  
683 Biol.*, 22(2), 613–626, doi:10.1111/gcb.13094, 2016.
- 684 Wilson, H. F. and Xenopoulos, M. a.: Effects of agricultural land use on the composition of fluvial dissolved organic matter,  
685 *Nat. Geosci.*, 2(1), 37–41, doi:10.1038/ngeo391, 2009.
- 686 Winter, C., Hein, T., Kavka, G., Mach, R. L. and Farnleitner, A. H.: Longitudinal changes in the bacterial community  
687 composition of the Danube River: A whole-river approach, *Appl. Environ. Microbiol.*, 73(2), 421–431,  
688 doi:10.1128/AEM.01849-06, 2007.
- 689 Yoon, T. K., Jin, H., Oh, N.-H. and Park, J.-H.: Technical note: Assessing gas equilibration systems for continuous  $p\text{CO}_2$   
690 measurements in inland waters, *Biogeosciences*, 13(13), 3915–3930, doi:10.5194/bg-13-3915-2016, 2016.
- 691 Yoon, Y., Ryu, J., Oh, J., Choi, B.-G. and Snyder, S. A.: Occurrence of endocrine disrupting compounds, pharmaceuticals,  
692 and personal care products in the Han River (Seoul, South Korea), *Sci. Total Environ.*, 408(3), 636–643,  
693 doi:10.1016/j.scitotenv.2009.10.049, 2010.
- 694 Zsolnay, A., Baigar, E., Jimenez, M., Steinweg, B. and Saccomandi, F.: Differentiating with fluorescence spectroscopy the



695 sources of dissolved organic matter in soils subjected to drying, *Chemosphere*, 38(1), 45–50, doi:10.1016/S0045-

696 6535(98)00166-0, 1999.

697

698 **Figure captions**

699 **Fig. 1.** Sampling locations in the Han River basin, South Korea. The locations of major dams along the midstream reach and  
700 waste water treatment plants (WWTPs) along the downstream reach are also indicated by different symbols. Note that a red  
701 triangle termed “mainstem” indicates the location of the mainstem sample used for the second incubation.

702 **Fig. 2.** Initial  $p\text{CO}_2$  levels measured in situ and BDOC concentrations measured with the filtered and unfiltered samples  
703 during 7 day laboratory incubation. BDOC concentrations represent the means of three replicate measurements ( $\pm$  one  
704 standard deviation), whereas one spot measurement of  $p\text{CO}_2$  was conducted at each site except site Urban 3. Asterisks above  
705 the site name indicate significant ( $P < 0.05$ ) differences in the BDOC concentration between the filtered and unfiltered  
706 samples.

707 **Fig. 3.** Spatial variation in DOM optical indices measured for the pre-incubation samples from up-, mid-, and downstream  
708 reaches and urban tributaries of the Han River. Error bars indicate a standard deviation of the measurements at three sites in  
709 each group. Significant differences among the up-, mid-, and downstream reaches and urban tributary sites are indicated by  
710 the different letters above the error bar.

711 **Fig. 4.** Relationships between BDOC and  $p\text{CO}_2$ , DOC concentration, or optical indices. All significant regressions at  $P <$   
712 0.05 except HIX and  $\text{SUVA}_{254}$  are indicated by dotted lines through the plots.

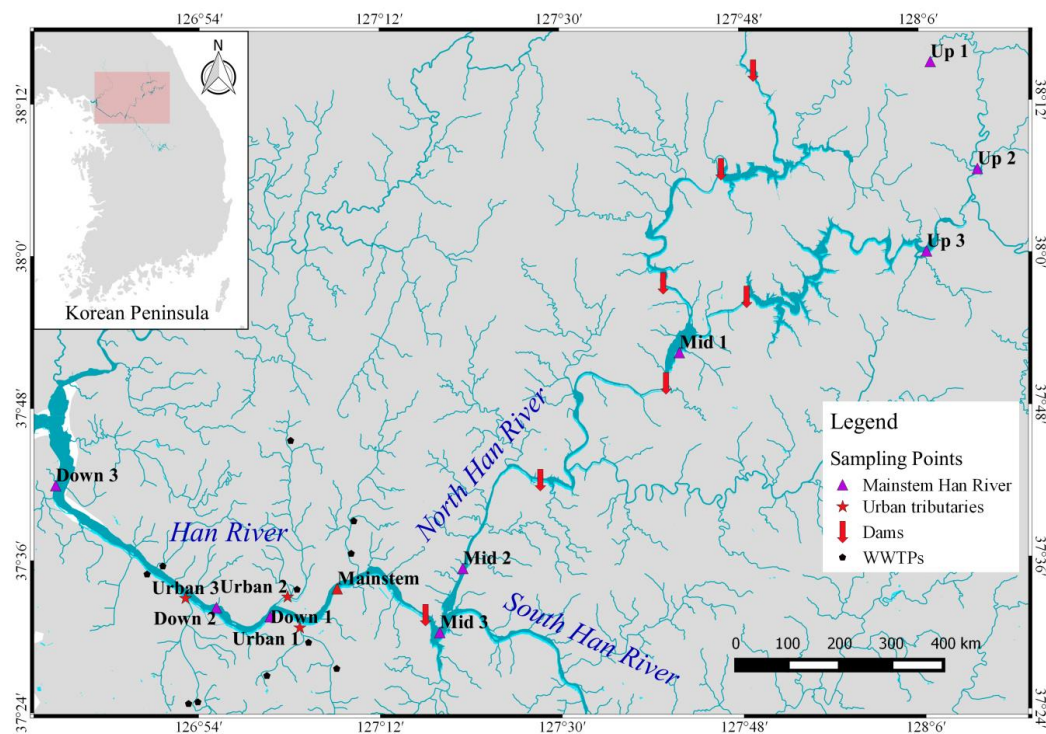
713 **Fig. 5.** Short-term dynamics of DOC and  $\text{CO}_2$  during the 5 day incubation of unfiltered water samples including a mainstem  
714 and a tributary of the Han River and their mixture (1:1); (a) DOC concentrations ( $\text{mg C L}^{-1}$ ) and cumulative BDOC  
715 concentrations ( $\text{mg C L}^{-1}$ ); (b) DOC concentrations ( $\text{mg C L}^{-1}$ ) and %BDOC relative to the initial DOC; (c) dissolved  $\text{CO}_2$   
716 concentration ( $\text{mg C L}^{-1}$ ); (d) cumulative production of  $\text{CO}_2$  ( $\text{mg C L}^{-1}$ ). The mainstem and tributary samples were collected  
717 from sites “mainstem” and “Urban 2” marked in Figure 1, respectively.

718 **Fig. 6.** Initial and differential fluorescence EEMs obtained at 0 h, 1 h, 1 day, 3 day, and 5 day during the 5 day incubation of  
719 unfiltered water samples; including a mainstem sample (first and second panels) and a tributary sample (third and fourth  
720 panels) of the Han River and their 1:1 mixture (fifth and sixth panels). Positive and negative values in differential EEMs  
721 indicate production and consumption of DOM components, respectively.

722 **Fig. 7.** Van Krevelen diagrams of identified molecular formulas showing changes in the peak intensity relative to the initial  
723 value during a 5 day incubation of unfiltered water samples from (a) a mainstem and (b) a tributary site of the Han River.  
724 Red and blue symbols represent molecular formulas that increased (termed “production”) and decreased (termed



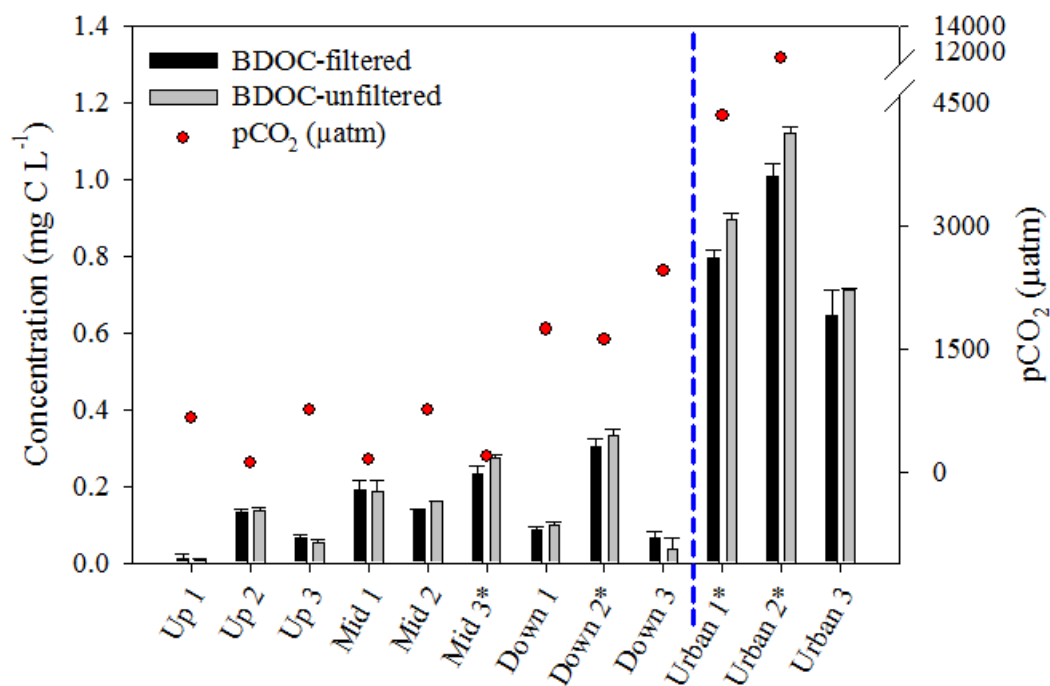
725 “consumption”) in peak intensity following the 5-day incubation, respectively.



726

727 Fig. 1

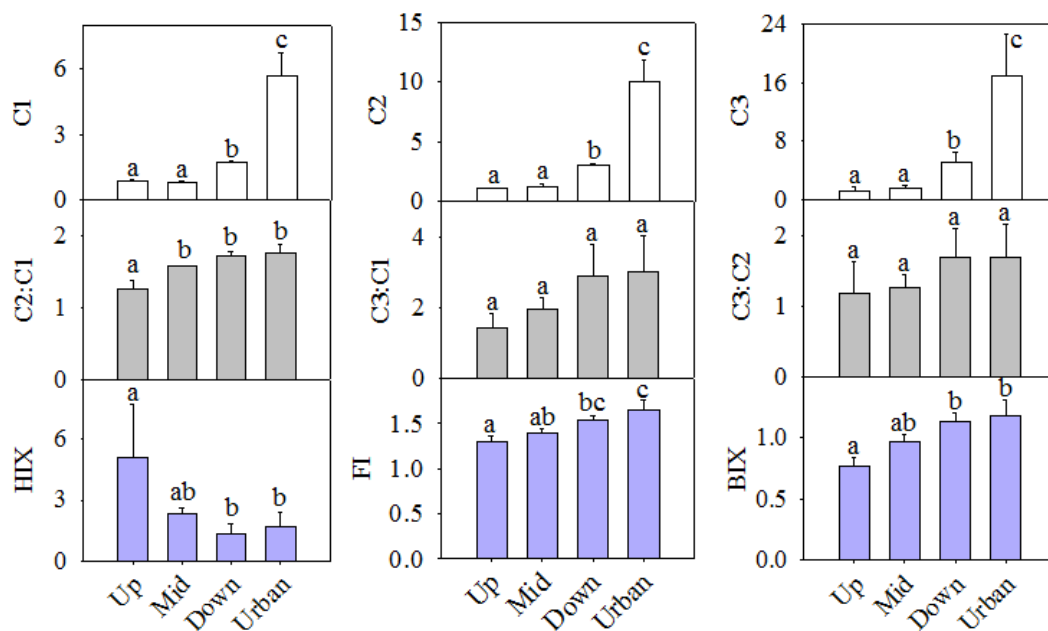
728



729

730 Fig. 2

731

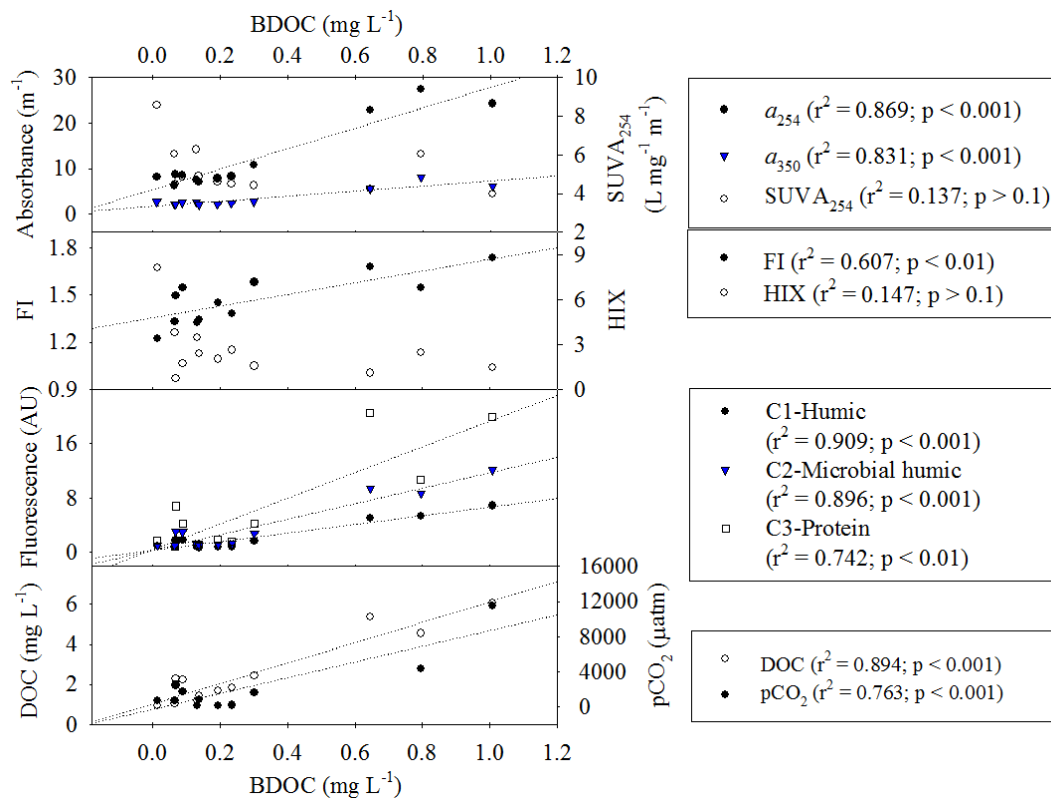


732

733

734 Fig. 3

735

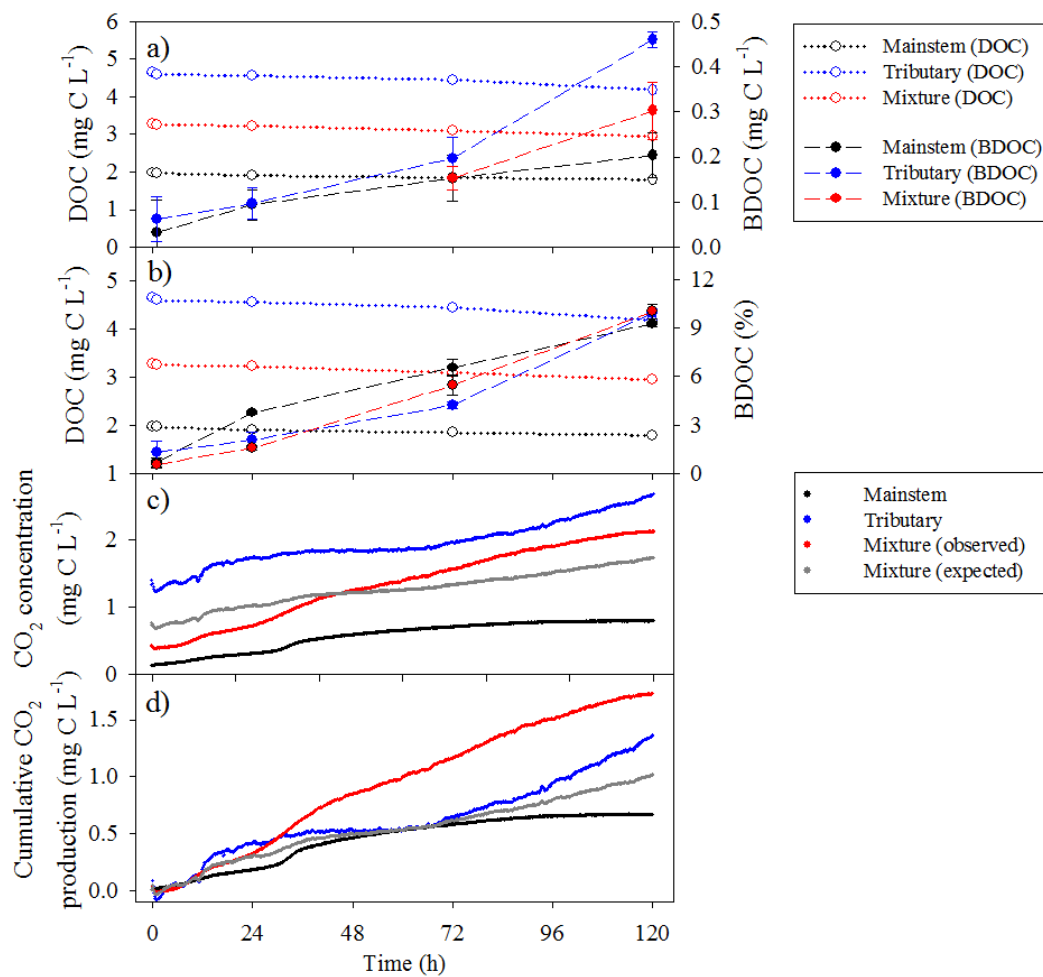


736

737

738 Fig. 4

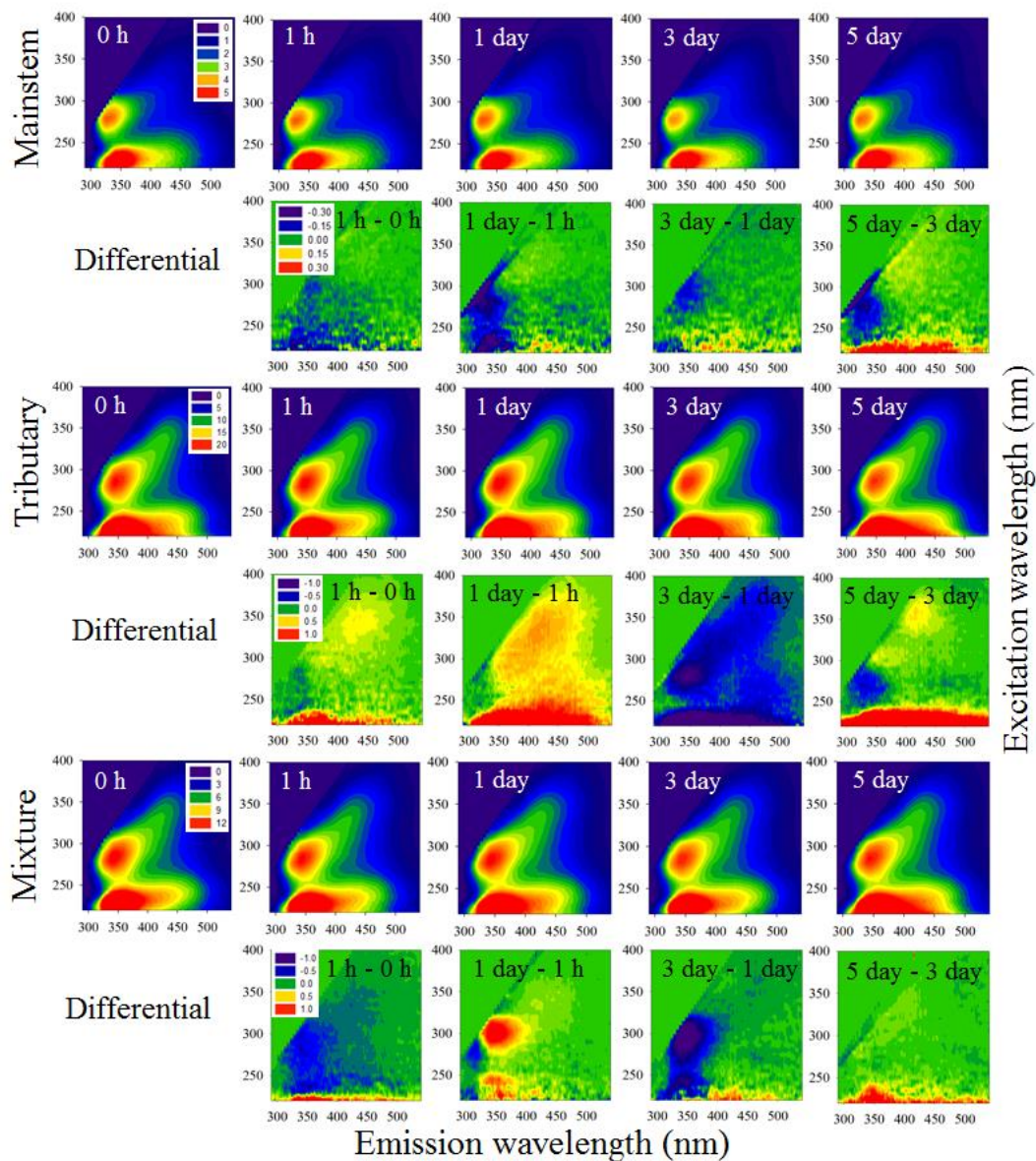
739



740

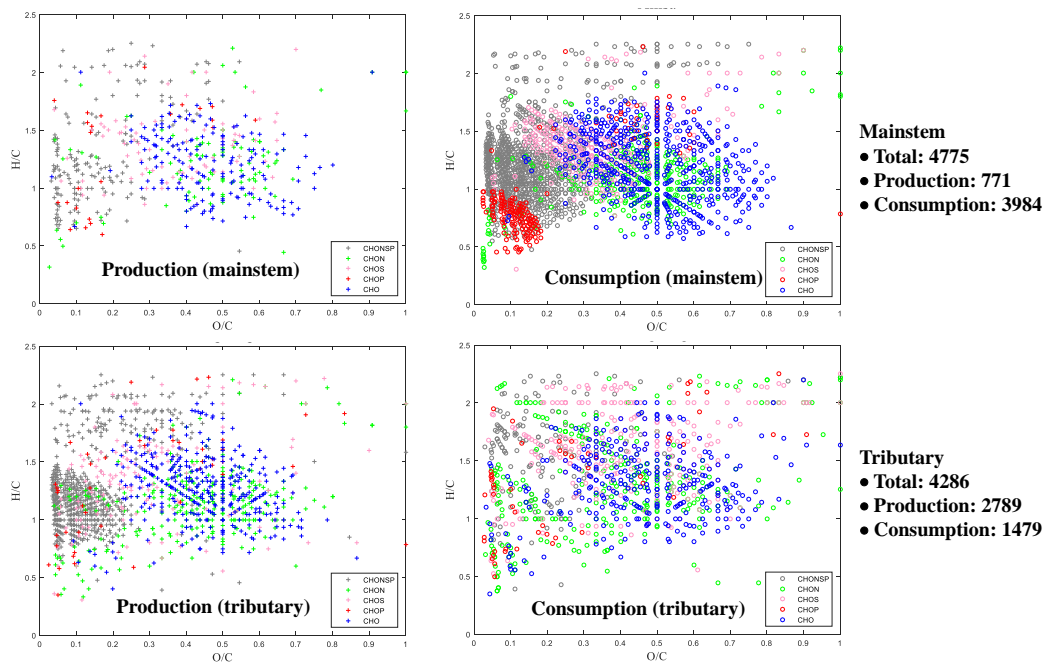
741 Fig. 5

742



743

744 Fig. 6



745

746 Fig. 7